

OK P

NASA TECHNICAL NOTE



NASA TN D-2672

NASA TN D-2672

PROPERTY OF:  
AMPTIAC LIBRARY

DISTRIBUTION STATEMENT A  
Approved for Public Release  
Distribution Unlimited

59088

INVESTIGATION OF THE  
ELASTIC-PLASTIC STRESS STATE  
AROUND A REINFORCED  
OPENING IN A SPHERICAL SHELL

*by Albert Kaufman and David A. Spera*

*Lewis Research Center*

*Cleveland, Ohio*

20010907 037

INVESTIGATION OF THE ELASTIC-PLASTIC STRESS STATE AROUND  
A REINFORCED OPENING IN A SPHERICAL SHELL

By Albert Kaufman and David A. Spera

Lewis Research Center  
Cleveland, Ohio

NATIONAL AERONAUTICS AND SPACE ADMINISTRATION

---

For sale by the Office of Technical Services, Department of Commerce,  
Washington, D.C. 20230 -- Price \$1.00

# INVESTIGATION OF THE ELASTIC-PLASTIC STRESS STATE AROUND A REINFORCED OPENING IN A SPHERICAL SHELL

by Albert Kaufman and David A. Spera

Lewis Research Center

## SUMMARY

A study was made to correlate theoretical stresses and strains in a <sup>A</sup> pressure vessel having a reinforced opening with experimental data obtained for progressive stages of elastic-plastic deformation up to the point of failure. The pressure vessel consisted of a hemispherical dome 12 inches in diameter with a wall thickness of 0.060 inch and a reinforced opening 1 inch in diameter and was machined from 6061 aluminum. The reinforcement was an integrally machined ring 1.70 inches in outer diameter and 0.300 inch thick. In general, there was good agreement between the experimental data and the theoretical results based on true stress - conventional strain data and modified shell dimensions. The conclusion was drawn that the theoretically computed elastic-plastic stresses can be used with the true ultimate tensile strength of the shell material to give a reasonably accurate prediction of the burst pressure. Also, the elastic stress-concentration factor can be used together with the true ultimate tensile strength to give a conservative approximation of this burst pressure. [Biaxial tests]

## INTRODUCTION

Reinforcements are utilized around the openings in shells to reduce stresses caused by the removal of material from the parent structure. In this study, experimental and theoretical analyses of the elastic-plastic stress state around a reinforced opening in a spherical pressure vessel were obtained for progressive stages of deformation up to failure.

The most common measure of the effectiveness of an opening reinforcement is an experimental or theoretical elastic stress-concentration factor. Usually this factor is combined with the yield strength of the shell material to determine the pressure load at which incipient local plastic flow takes place. [An ideal reinforcement is one in which the]

pressure at which local yielding (plastic flow) occurs is the same as if the pressure vessel did not contain an opening or reinforcement.

Elastic stress-concentration factors have been investigated for apex openings in biaxially stressed plates (refs. 1 to 5). [A small amount of local plastic flow can very significantly reduce the stress-concentration factor] (ref. 6); therefore, the elastic stress-concentration factor may result in an unduly conservative prediction of the ability of vessels with reinforced openings to withstand internal-pressure loadings. It therefore appears that an elastic-plastic stress analysis is required to provide a more realistic evaluation of the effectiveness of the reinforcement.

References 7 and 8 present numerical analyses of a continuous elastic-plastic shell that can be modified to treat the problem of a reinforced opening. Reference 9 presents a numerical analysis that is directly applicable to the reinforced opening problem. All of these theoretical methods are based on the von Mises yield criterion and associated flow rules and on the assumption of infinitesimal strains. In addition, shear deformations are neglected. The validity of these assumptions requires experimental verification for the case of the finite deformation of a shell that contains a discontinuity such as an opening reinforcement.

The purposes of this investigation are threefold: first, to evaluate the accuracy with which plasticity theory and a numerical shell analysis can predict the elastic-plastic stress and strain states in a discontinuous shell structure loaded to failure; second, to evaluate the validity of the elastic stress-concentration factor as a measure of the effectiveness of a reinforcement around an opening in a pressure vessel; third, to use these results to draw some preliminary conclusions about a method for predicting the burst pressure and the mode of failure for such a reinforced vessel.

Experimental strain data to the burst point were obtained from a hemispherical dome with a nominal diameter of 12 inches, a wall thickness of 0.060 inch, and a reinforced circular apex opening 1 inch in diameter. The reinforcement proportions were those of the most effective configuration for strengthening a hole in a biaxially stressed sheet with a stress field ratio of 1, as reported in reference 2. The strain data were correlated with results from a conventional elastic-edge-influence-coefficient analysis and the elastic-plastic shell analysis of reference 9 and are presented in this report.

## SYMBOLS

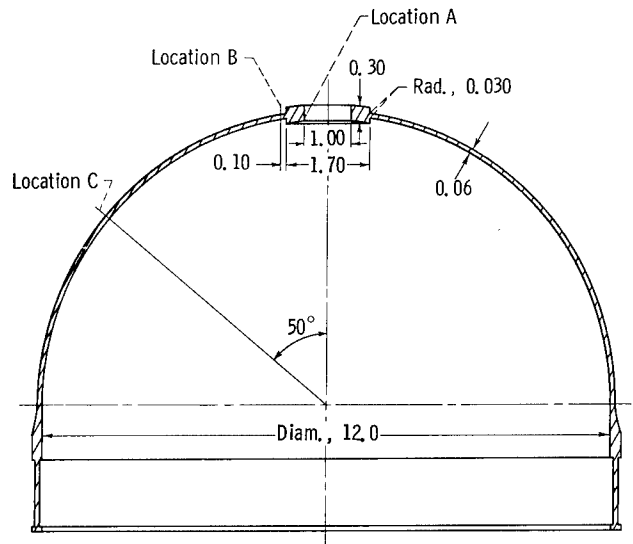
a	radius of dome, in.	$h, h'$	thickness of shell and ring, respectively
E	modulus of elasticity, psi	M	couple, lb-in. /in.
H, V	radial and axial stress re- sultants, lb/in.	p	pressure, lb/sq in.

r	radial coordinate, in.	H, M	caused by a unit radial force and meridional couple, respectively
$\bar{r}$	radial coordinate to centroid of ring, in.		
u	radial displacement, in.	o	original
$\beta$	meridional rotation, rad	max	maximum
$\delta, \theta$	influence coefficients for deflection and rotation, respectively	mem	membrane
$\epsilon$	strain, in./in.	p	caused by a unit internal pressure
$\nu$	Poisson's ratio	R, S	ring, shell
$\sigma$	stress, psi	t	transverse direction
$\bar{\sigma}$	true stress, psi	u	uniaxial test data
$\sigma_e$	effective stress, $\sqrt{\sigma_\phi^2 - \sigma_\phi \sigma_\theta + \sigma_\theta^2}, \text{ psi}$	y	yield
$\phi$	meridional slope, rad	$\zeta, \zeta_p$	transverse, transverse plastic
Subscripts:		$\theta, \theta_e, \theta_p$	circumferential, circumferential elastic, circumferential plastic
e	effective	$\phi, \phi_p$	meridional, meridional plastic
et, ep	effective total, effective plastic	1, 2	inner and outer circumference of reinforcement, respectively

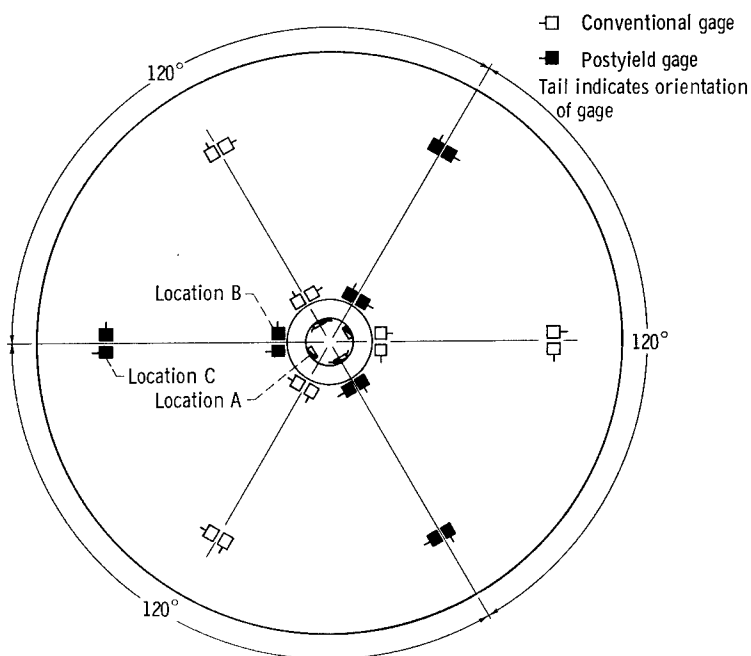
## EXPERIMENTAL APPARATUS AND PROCEDURE

### Test Specimen

The geometry of the hemispherical-dome test specimen is shown in figure 1. The dome had a nominal diameter of 12 inches, a wall thickness of 0.060 inch, and an apex opening 1 inch in diameter. The reinforcement ring was integrally machined to an outer diameter of 1.70 inches, a thickness of 0.30 inch, and had a 0.030-inch radius fillet at the junction with the shell. Fabrication tolerances were specified as  $\pm 0.002$  inch for the dome and ring diameters and  $\pm 0.001$  inch for the dome wall and ring thicknesses. The dome and four tensile coupons were cut from a billet of 6061-0 aluminum alloy and heat treated to the T6 condition prior to final machining.

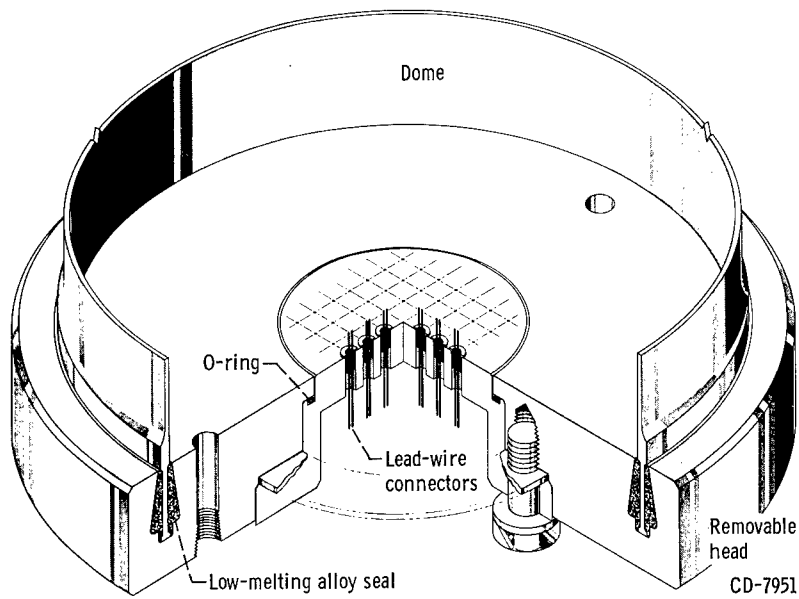


(a) Dome geometry.

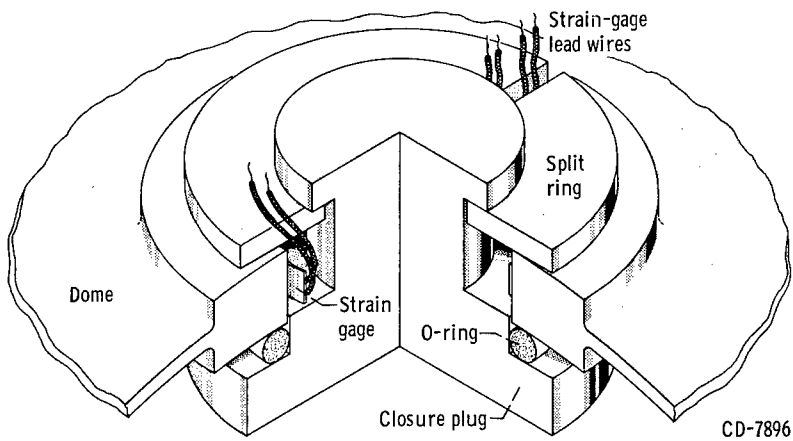


(b) Location and orientation of strain gages on inside and outside surfaces of shell and in hole

Figure 1. - Dome test specimen and strain-gage installation. All dimensions in inches.



(a) Dome base.



(b) Apex opening.

Figure 2. - Methods of closure of dome.

Figure 2(a) shows the method of closing the base of the dome. A removable head was attached and sealed with an alloy that melted at about 300<sup>o</sup> F, as described in reference 10. A cooling coil was wrapped around the dome to protect the strain gages from the heat during installation of the removable head. The apex opening of the dome was sealed by a stainless steel plug and a rubber O-ring, as shown in figure 2(b).

### Strain-Gage Installation

Two types of electrical resistance strain gages were used in this investigation. First, conventional Advance foil gages with 1/8-inch-square active elements were in-

stalled to measure strains below the elastic limit. These were replaced later by post-yield Advance gages of the same size to measure strains in the elastic-plastic range. The postyield gages that were used were found from tests to be less accurate than the conventional gages in the elastic range and were, therefore, not used to measure the elastic strains up to the yield point.

Twenty-eight conventional gages and 28 postyield gages were mounted at the locations indicated in figure 1(b). Two circumferentially oriented gages and two axially oriented gages were placed along the inner circumference of the reinforcing ring at location A. Three pairs of gages were installed on both the inside and outside surfaces of the shell with the gage centerlines 0.1 inch from the reinforcement ring (location B). Each pair consisted of meridionally and circumferentially oriented gages. Installations similar to location B were made at location C, approximately midway between the reinforcement and the end closure. Gages were bonded to the specimen with cyanoacrylate cement. Lead wires from the interior gages were brought through the tank base by pass-through connectors (fig. 2(a)). Lead wires from location A passed through the split ring in the closure plug assembly as shown in figure 2(b). A multichannel digital recorder utilizing a five-wire system was used to measure and tabulate the gage output.

## Testing Procedure

The dome was loaded by internal hydraulic pressure that was measured on Bourdon gages having a maximum error of 0.5 pound per square inch. In the elastic range, gage readings were taken at pressures of 0, 100, 200, 300, 400, 500, and 600 pounds per square inch. Each pressure increment resulted in a membrane stress increase of about 5000 pounds per square inch. The pressure was released after each reading, and a zero reading was again taken. A uniform time interval of 4 minutes was maintained between readings to minimize viscoelastic effects, and a duplicate run was made. The maximum difference between the two runs was less than 1 percent.

Following completion of testing in the elastic range, the dome was reinstrumented with postyield gages and pressurized to burst. Data were taken in the course of this loading at pressures of 0, 600, 650, 700, 750, 800, 850, and 900 pounds per square inch. The load was held constant at each of these values only long enough to record readings from all 28 gages, in an effort to minimize the effects of creep, which were far more serious than viscoelastic effects in the plastic range. This time interval was somewhat under a minute. Bursting of the specimen occurred at a pressure of 935 pounds per square inch about 10 minutes after the postyield loading was begun.

## Reduction of Data

Data from the conventional gages were entered into a computer program for the reduction of elastic-strain readings, which corrected them for zero drift and nonlinearity by the method of least mean squares and converted the readings to stresses and strains. The data from the two runs were averaged. Output data from the postyield gages were processed by a second program that used an iterative procedure to calculate the elastic and plastic components of the measured strains. By using a stress-strain curve based on the true stress and conventional strain test data obtained from the tensile coupons machined from the billet, stresses in the plastic range were calculated as explained in appendix A.

## THEORETICAL ANALYSIS

### Elastic State

Stresses in the shell prior to yielding were calculated by a standard edge-influence-coefficient technique and also by a numerical solution of the governing differential equations. The first method is explained in detail in appendix B, and the second was taken from reference 9.

Influence-coefficient analysis. - A number of methods are available for calculating the edge deformations in a shallow shell as a result of pressure and boundary loads. Galletly (ref. 4) analyzed three of these methods and recommended Esslinger's solution, in which the approximation  $\cot \varphi = 1/\varphi$  is made. This approximation is acceptable for values of the meridional slope  $\varphi$  up to about  $30^\circ$ , for which the error would be about 10 percent. Because of the local nature of the effects of boundary forces and moments in shells, significant values of  $\varphi$  would be limited to about  $30^\circ$  in a dome with an apex opening half-angle of about  $15^\circ$ . In the present investigation, the spherical dome contained an apex opening with a half-angle of about  $8^\circ$  as measured to the outside diameter of the reinforcement. Therefore, Esslinger's coefficients were applicable. Combined with the well-known ring-deformation equations (ref. 11), they yielded discontinuity forces and moments at the ring-shell junction, which in turn led to the elastic stresses.

Numerical analysis. - In an alternative elastic-state analysis based on reference 9, the reinforcement was treated as a short spherical segment. Equations of equilibrium and compatibility for both the reinforcement and the dome segments were reduced to two second-order ordinary differential equations. The independent variable in these equations was the meridional slope  $\varphi$ . The two dependent variables were the change in meridional slope and the radial stress resultant. These differential equations were based on

the usual thin-shell assumptions, namely, that transverse stresses and shearing strains are negligible and that wall thicknesses are much smaller than radii of curvature.

Boundary conditions on the basic differential equations were as follows. At the inner circumference of the reinforcement, the radial stress resultant vanished, while the axial stress resultant and the meridional couple together were statically equivalent to the closure-plug load as applied at the centerline of the O-ring a small distance from the edge (fig. 2(b)). At the common boundary between the reinforcement segment and the shell segment, corresponding edge forces and deformations in the two segments were made equal. Finally, at the outer boundary of the dome, which was assumed to lie in a membrane region, the transverse stress resultant and the meridional couple vanished.

The reinforcement and the dome meridians were subdivided into equal increments 0.05 inch in length. The two differential equations were expressed in finite-difference form, and a numerical integration technique, which is given in detail in reference 9, was applied to solve them. The meridional-slope changes and the radial stress resultants thus obtained were used to determine the elastic stress and strain states throughout the shell and reinforcing ring.

### Elastic-Plastic State

The numerical analysis of reference 9 was also applied to the shell in the elastic-plastic state. As explained in appendix A, the deformation theory of plasticity and the method of successive approximations were used to determine the plastic components of strain. The solution of the basic differential equations for each approximation was identical to the elastic-state solution. Boundary and junction conditions were modified to include the effects of plastic strain and were then incorporated into the numerical solution, as explained previously.

The elastic-plastic analysis was applied to the reinforced dome under conditions ranging from incipient plastic flow to burst. It was therefore necessary to make some provision for the small but finite middle surface strains, which would certainly be present under this wide range of loads. This was done by assuming that, at a given pressure, the curvature and the wall thickness throughout the shell were equal to the curvature and the wall thickness in the membrane region of the dome. These latter dimensions are calculated in appendix C (see table I, p. 21). The true effective stress - conventional effective strain curve that was based on the data in table I is shown in figure 3 together with an exponential curve fit. This use of the instantaneous membrane dimensions together with true stress - conventional strain data ensured that the correct theoretical stress - strain - pressure relations would exist in the membrane region of the dome even with small finite strains.

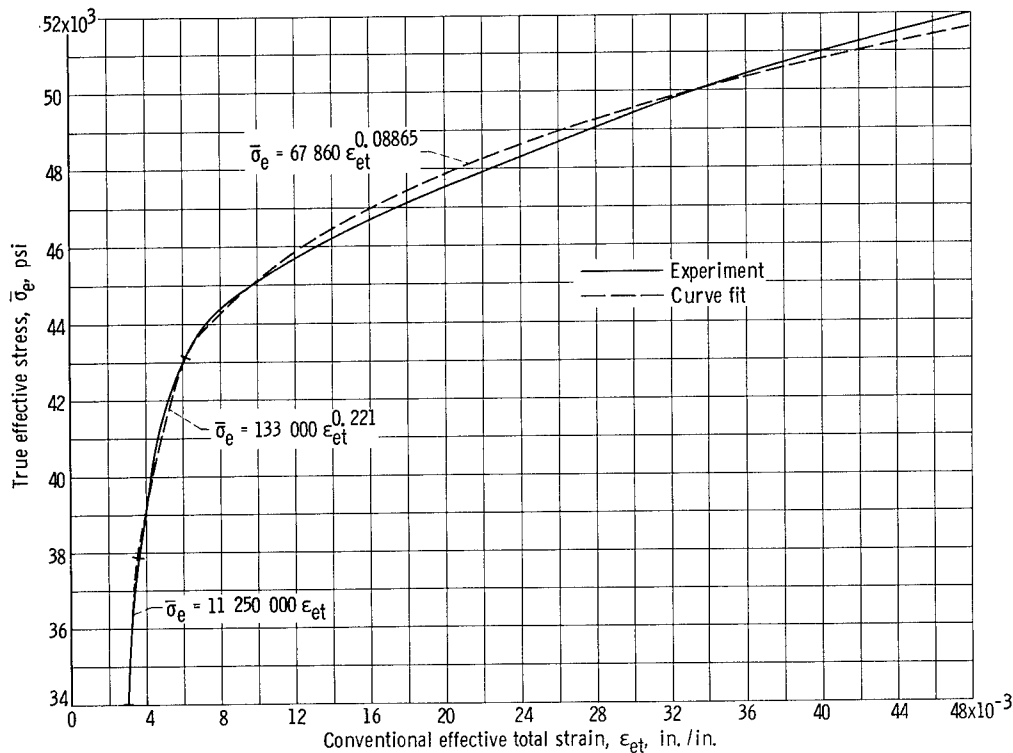


Figure 3. - Effective stress - effective total strain relations.

## RESULTS AND DISCUSSION

### Elastic State

The results of the experimental and theoretical elastic-stress analyses of the dome test specimen are compared in figure 4. Stresses are normalized with respect to the nominal membrane stress in the shell. Circumferential and meridional stresses that were calculated by the numerical method of reference 9 are presented for both inside and outside surfaces along a meridian. Experimental data are represented by rectangular symbols whose dimensions indicate the gage length and the scatter. Agreement between the experimental data and the theoretical stresses is generally good.

The maximum theoretical stress occurred on the inside surface of the shell at the ring-shell junction. At this location the nondimensional meridional stress was 1.42 from calculations based on either reference 9 or the influence-coefficient analysis, which is explained in appendix B. This stress concentration was caused mainly by the discontinuity moment at the junction because the effective stress-concentration factor of the middle surface was 0.975.

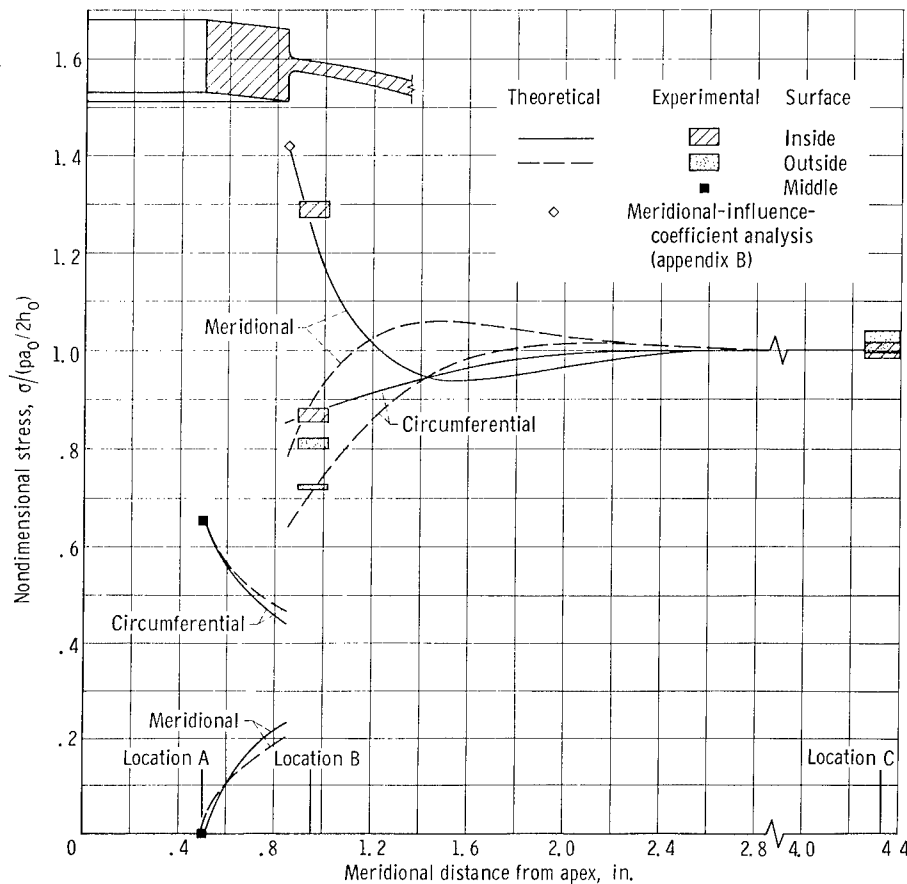


Figure 4. - Experimental and theoretical elastic stress.

### Elastic-Plastic State

Curves of strain in the dome as a function of internal pressure are shown in figure 5 for locations B (near the ring-shell junction) and C (in the membrane region). The experimental data are shown for pressures above 600 pounds per square inch, the pressure for incipient plastic flow, and terminate at the last pressure at which data were taken before the strains went out of the range of the measuring equipment. The experimental burst pressure is also indicated. Most of the experimental and theoretical data become increasingly nonlinear at pressures above 800 pounds per square inch and increase so rapidly as to indicate an instability condition above 900 pounds per square inch. For both the inside surface (fig. 5(a)) and the outside surface (fig. 5(b)) at location B near the reinforcement, the theoretical strains are substantially lower than the measured strains. The greatest discrepancy between experiment and theory is at the outside surface at location B, as is shown in figure 5(b) by the meridional strain curves. The theoretical analysis predicted a strain that decreased at pressures above 800 pounds per square inch

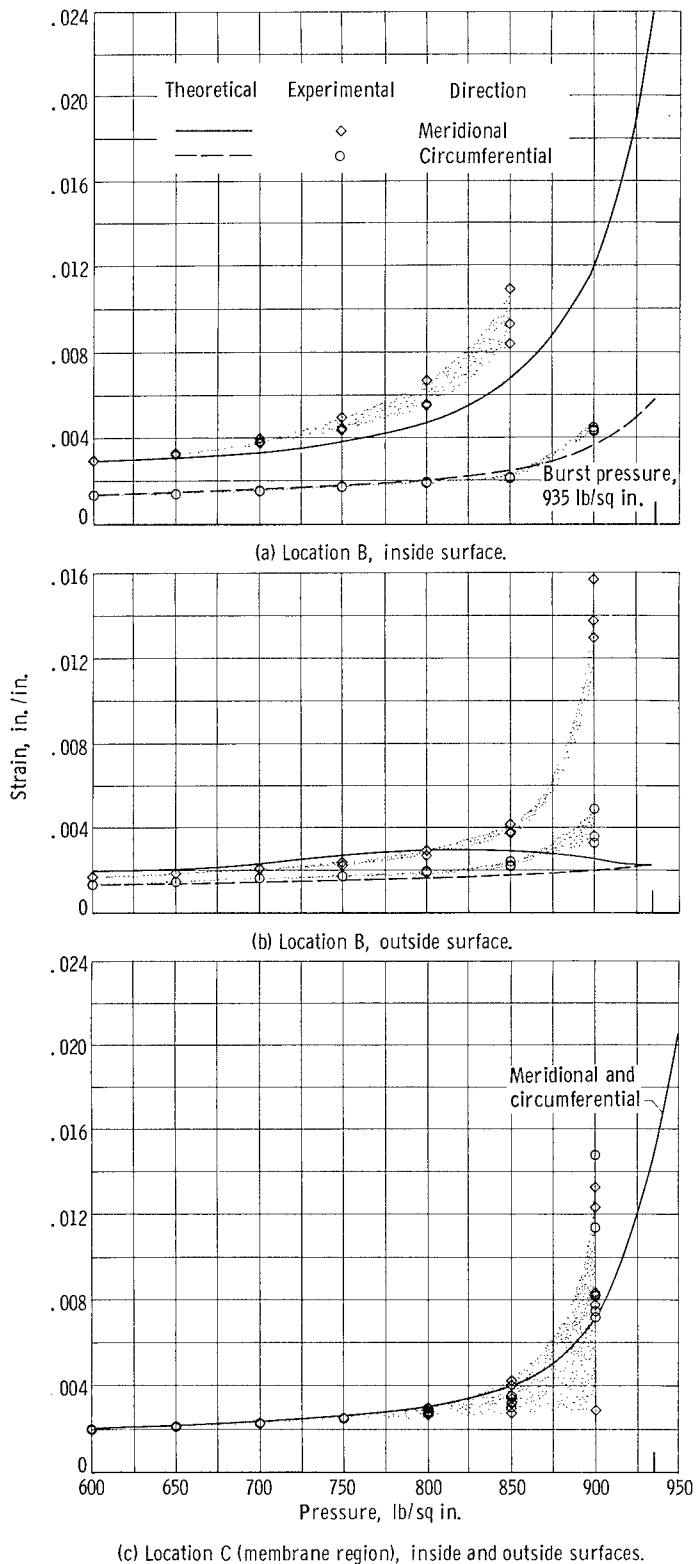


Figure 5. - Experimental and theoretical strains in elastic-plastic state.

and remained in the elastic state, while the measured strains actually increased and experienced substantial plastic flow. In the membrane region (fig. 5(c)) the wide scatter band includes data from 12 gages oriented in meridional and circumferential directions on both inside and outside surfaces in the nominal membrane region of the shell. This scatter was probably caused mainly by distortion of the dome and nonuniform reduction in wall thickness with increasing pressure.

In figure 6 experimental and theoretical results are correlated on the basis of true stress as a function of pressure. Because stresses increase slowly with increasing strain in the plastic state, agreement between experimental and theoretical results is better for stresses than for strains. The experimental burst pressure and the theoretical membrane burst pressure from table I (p. 21) are also indicated.

Both the experimental and the theoretical data presented in figure 6 show that the material at location A remains elastic up to the burst pressure. The theoretical solution shows a tensile instability in the membrane region at a pressure of 969 pounds per square inch. The experimental data for location C show that the stress field ratio of 1 was not maintained as plastic flow increased. At a pressure of 900 pounds per square inch the circumferential stresses were

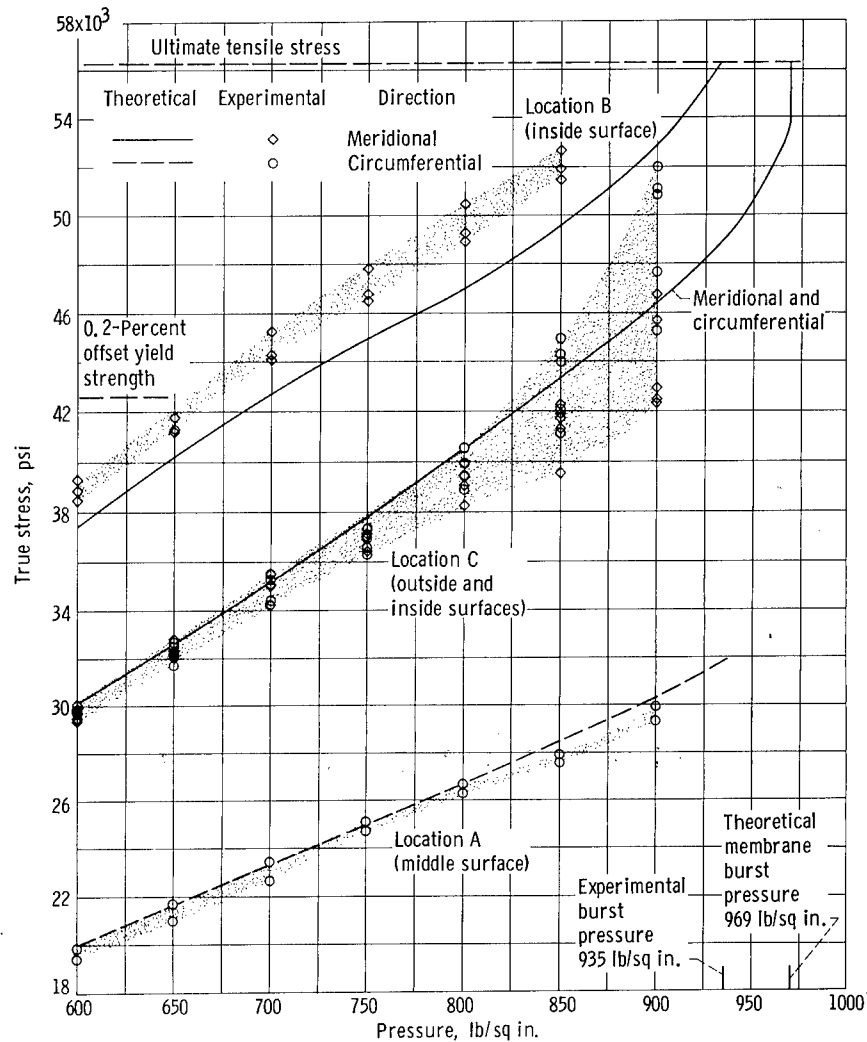
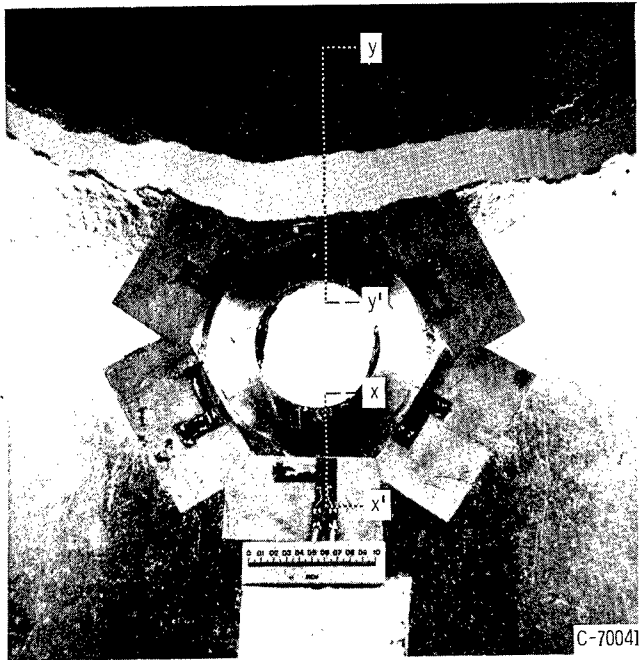


Figure 6. - Experimental and theoretical stresses in elastic-plastic state.

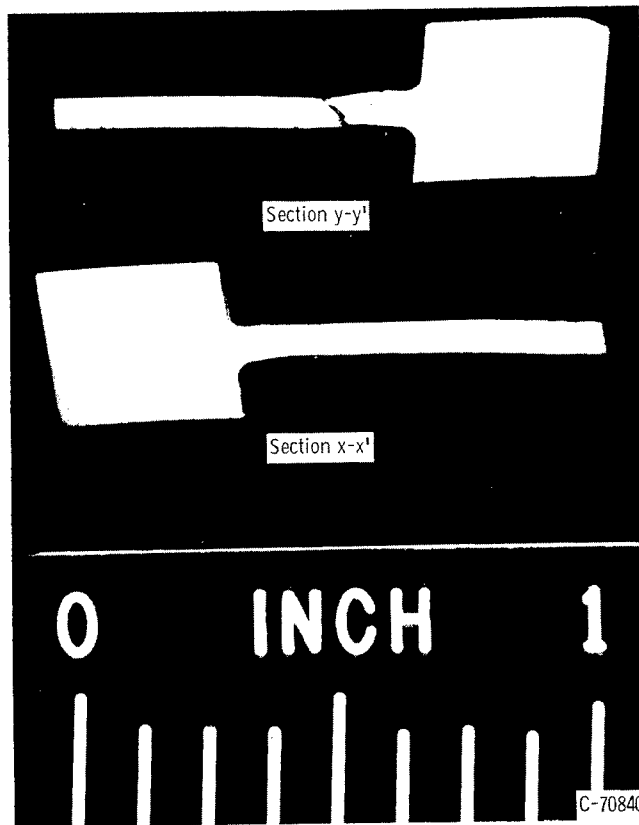
generally higher than the meridional stresses. The maximum measured stresses on the inside surface at location B in the meridional direction were higher than those predicted for this location. The theoretical curve for this location reached the ultimate tensile strength of the material at a pressure of 933 pounds per square inch, however, or only 0.2 percent below the experimental burst pressure of 935 pounds per square inch.

*(burst test)* **Burst Condition**

A view of the dome fracture and meridional sections through the junction region are shown in figure 7. The failure apparently originated on the inside surface approximately 0.1 inch from the ring-shell junction. The rough surface of the dome apparent in fig-



(a) View of fracture from inside dome.



(b) Meridional sections through junction region.

Figure 7. - Apex region after burst.

ure 7(a) was caused by high plastic flow. The specimen had an initial root mean square surface finish of 32 microinches.

The sectional views in figure 7(b) show a definite necking in the dome material a small distance from the ring-shell junction. There is no apparent thinning at the junction itself, however, because of the transverse restraint of the ring and fillet. This restraint, together with the slight thickening of the dome wall near the root of the fillet, probably caused the maximum stress to be displaced from the fillet to the point at which the shell wall assumed a uniform thickness.

The experimental burst results and the theoretical maximum stresses are correlated in figure 8. The stresses are nondimensionalized with respect to the nominal membrane stress for the dome computed from the original shell dimensions. If no fillet had been present, the highest stress would have occurred at the ring-shell junction on the inside surface of the shell. When a small fillet is present, it is reasonable to assume that the critical location is transferred to the end of the fillet.

The elastic stress-concentration factor for the end of the fillet on the inside surface is 1.36 from the analysis of reference 9. On the basis of the ultimate tensile strength, this would lead to a prediction of a burst pressure of 813 pounds per square inch, which is 13 percent below the experimental burst pressure.

The nondimensional elastic-plastic stress curve from the analysis of reference 9

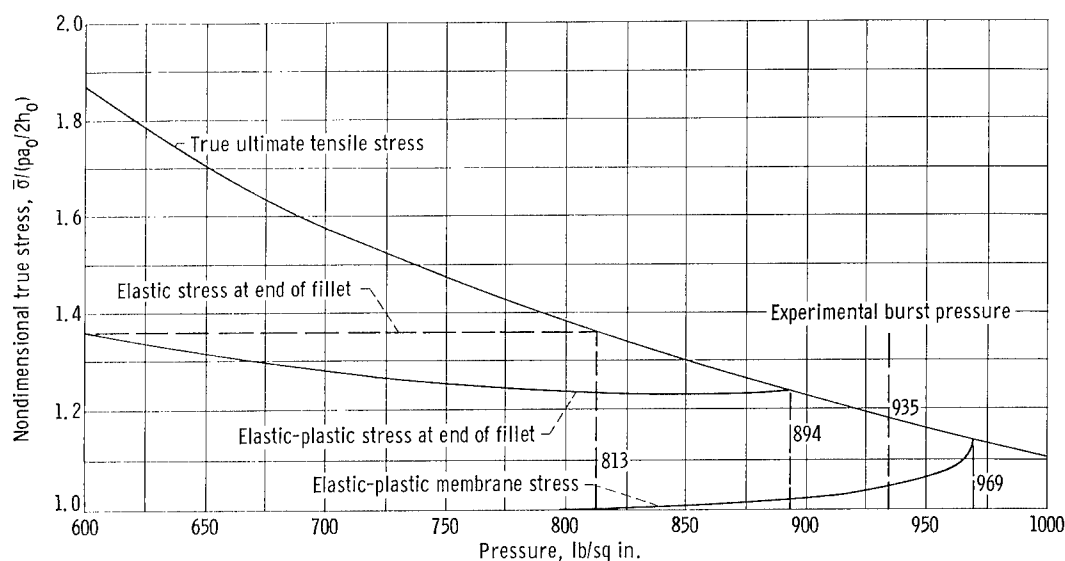


Figure 8. - Correlation of experimental burst results and theoretical predictions for burst pressure.

gives a predicted burst pressure of 894 pounds per square inch, about 4 percent below the experimental burst pressure. The predicted burst pressure for the membrane region of the dome in which failure would occur through tensile instability (table I, p. 21) is 969 pounds per square inch, about 4 percent above the experimental burst pressure.

[Based on the maximum stress failure theory, the elastic stress-concentration factor gives the minimum predicted burst strength of the shell, while the elastic-plastic membrane instability analysis gives the theoretical maximum pressure the shell can withstand.] The difference between these two values would determine whether it would be worthwhile to go through an elastic-plastic shell analysis. The membrane stress curve for a shell without a hole intersects the ultimate tensile stress curve at a nondimensional stress of 1.14. This is the elastic stress-concentration factor that the dome could tolerate without any deleterious effect.

## CONCLUSIONS

The following general conclusions are drawn from the results of this investigation of the elastic-plastic stress and strain states in a pressurized spherical shell with an apex opening reinforced by an integrally machined ring:

1. The numerical shell analysis and the shallow-shell edge-influence-coefficient analysis give identical results for the elastic stress-concentration factor in a shell containing a discontinuity such as a reinforced opening.

2. Correlation between experimental and theoretical stresses and strains in the elastic state is very good.

3. The deformation theory of plasticity and the method of successive approximations can be combined with a numerical shell analysis to calculate elastic-plastic stresses that are generally in good agreement with experimental results.

4. The elastic-plastic stresses based on true stress data and the instantaneous membrane shell dimensions could be used with the true ultimate tensile strength of the shell material to give a reasonably accurate prediction of the burst pressure in a shell containing a discontinuity.

5. The elastic stress-concentration factor may be used in conjunction with the true ultimate tensile stress for a ductile material to give a conservative approximation of the burst pressure. The discrepancy between the experimental burst pressure and the burst pressure calculated from the elastic stress-concentration factor was 13 percent in this investigation.

Lewis Research Center,  
National Aeronautics and Space Administration,  
Cleveland, Ohio, December 10, 1964.

## APPENDIX A

### ELASTIC-PLASTIC STRESS AND STRAIN EQUATIONS

Derivations of equations similar to or identical with the following equations are presented in detail in reference 12 and will not be repeated here. The stress and strain equations are

$$\epsilon_{et} = \frac{\sqrt{2}}{3} \sqrt{(\epsilon_{\varphi} - \epsilon_{\theta})^2 + (\epsilon_{\theta} - \epsilon_{\zeta})^2 + (\epsilon_{\zeta} - \epsilon_{\varphi})^2} \quad (\text{A1a})$$

$$\epsilon_{ep} = \epsilon_u - \frac{\sigma_u}{E} = \begin{cases} 0 & \text{for } \sigma_e \leq \sigma_y \\ \epsilon_{et} - \frac{2(1+\nu)}{3} \frac{\sigma_e}{E} & \text{for } \sigma_e > \sigma_y \end{cases} \quad (\text{A1b})$$

in which the subscript u indicates the results of a uniaxial tensile test, and the effective stress  $\sigma_e$  is a known function of  $\epsilon_{et}$  as determined by a curve fit of experimental data (fig. 3). The plastic components of strain are then given as

$$\epsilon_{\varphi p} = \frac{\epsilon_{ep}}{3\epsilon_{et}} (2\epsilon_{\varphi} - \epsilon_{\theta} - \epsilon_{\zeta}) \quad (\text{A2a})$$

$$\epsilon_{\theta p} = \frac{\epsilon_{ep}}{3\epsilon_{et}} (2\epsilon_{\theta} - \epsilon_{\zeta} - \epsilon_{\varphi}) \quad (\text{A2b})$$

$$\epsilon_{\zeta p} = -(\epsilon_{\varphi p} + \epsilon_{\theta p}) \quad (\text{A2c})$$

The total transverse strain is

$$\epsilon_{\zeta} = -\frac{1}{1-\nu} \left[ \nu(\epsilon_{\varphi} + \epsilon_{\theta}) + (1-2\nu)(\epsilon_{\varphi p} + \epsilon_{\theta p}) \right] \quad (\text{A3})$$

Finally

$$\sigma_{\varphi} = \frac{E}{1-\nu^2} \left[ (\epsilon_{\varphi} - \epsilon_{\varphi p}) + \nu(\epsilon_{\theta} - \epsilon_{\theta p}) \right] \quad (\text{A4a})$$

$$\sigma_{\theta} = \frac{E}{1 - \nu} \left[ (\epsilon_{\theta} - \epsilon_{\theta p}) + \nu(\epsilon_{\varphi} - \epsilon_{\varphi p}) \right] \quad (A4b)$$

$$\sigma_e = \sqrt{\sigma_{\varphi}^2 - \sigma_{\varphi} \sigma_{\theta} + \sigma_{\theta}^2} \quad (A4c)$$

The successive approximation technique for reducing experimental strain data in the elastic-plastic state is as follows. The measured total strains  $\epsilon_{\varphi}$  and  $\epsilon_{\theta}$  are combined with an assumed total transverse strain  $\epsilon_{\zeta}$  in equation (A1a) to produce a trial value of the equivalent total strain  $\epsilon_{et}$ . By using this trial value, first approximations to the equivalent plastic strain  $\epsilon_{ep}$  and the individual plastic strains  $\epsilon_{\varphi p}$  and  $\epsilon_{\theta p}$  can be calculated by using equations (A1b) and (A2). A second approximation to the transverse strain  $\epsilon_{\zeta}$  is then calculated from equation (A3), and the procedure is repeated until the desired degree of convergence is obtained. Stresses are then calculated by using equations (A4).

A similar procedure is used in the shell analysis of reference 9. In this analysis, the basic differential equations that describe the conditions of equilibrium and compatibility of deformation throughout the shell contain the plastic strain terms  $\epsilon_{\varphi p}$  and  $\epsilon_{\theta p}$ . For a first approximation, these terms are set equal to zero throughout the shell. Solution of the basic differential equations then yields the elastic-state strains. These strains are substituted into equation (A1a), and the resulting value of  $\epsilon_{et}$  is used to calculate  $\epsilon_{ep}$  and a second approximation to the plastic strains  $\epsilon_{\varphi p}$  and  $\epsilon_{\theta p}$ . The basic differential equations are re-solved with these improved plastic flow terms, and the process is repeated until convergence is reached. Stresses are then computed by means of equations (A4).

## APPENDIX B

### INFLUENCE-COEFFICIENT ANALYSIS

As shown by figure 9, compatibility of deformations at the junction of the ring and shell requires that

$$\left. \begin{aligned} u_R &= u_S \\ \beta_R &= \beta_S \end{aligned} \right\} r = r_2 \quad (B1a)$$

In influence-coefficient notation, equations (B1a) become

$$\left. \begin{aligned} \delta_{R,H} \left( \frac{pa}{2} \cos \varphi_2 + H_2 \right) + \delta_{R,M} M_R &= \delta_{S,H} H_2 + \delta_{S,M} M_2 + \delta_{S,p^p} \\ \theta_{R,H} \left( \frac{pa}{2} \cos \varphi_2 + H_2 \right) + \theta_{R,M} M_R &= \theta_{S,H} H_2 + \theta_{S,M} M_2 + \theta_{S,p^p} \end{aligned} \right\} \quad (B1b)$$

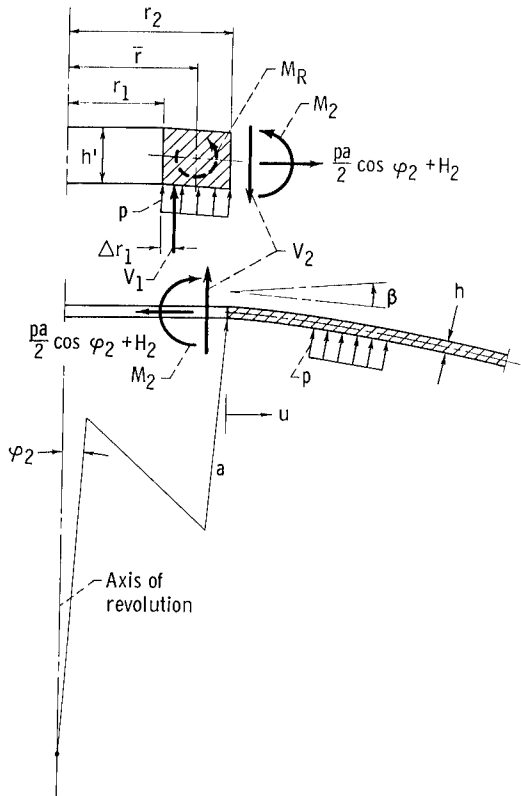


Figure 9. - Force diagram for influence-coefficient analysis.

The closure plug load  $V_1$  and the axial stress resultant  $V_2$  are

$$\left. \begin{aligned} V_1 &= \frac{pr_1}{2} \frac{r_1}{r_1 + \Delta r_1} \\ V_2 &= \frac{pr_2}{2} \end{aligned} \right\} \quad (B2)$$

The resultant twisting moment on the ring, referred to the centroid of its cross section, is then

$$M_R = \frac{1}{\bar{r}} \left[ r_2 M_2 - (r_1 + \Delta r_1)(\bar{r} - r_1 - \Delta r_1) V_1 - r_2(r_2 - \bar{r}) V_2 \right]$$

For the dimensions shown in figure 1

$$M_R = 1.2593 M_2 - 0.1145 p \quad (B3)$$

From reference 11, the ring influence coefficients for  $E = 10^7$  pounds per square inch and  $\nu = 0.333$  inch per inch are

$$\left. \begin{aligned} \delta_{R,H} &= \frac{r_2}{Eh'} \left( \frac{r_2^2 + r_1^2}{r_2^2 - r_1^2} - \nu \right) = 4.887 \times 10^{-7} \text{ in. / (lb/in.)} \\ \theta_{R,M} &= \frac{12\bar{r}}{E(h')^3 \ln\left(\frac{r_2}{r_1}\right)} = 565.4 \times 10^{-7} \text{ rad / ((lb-in.) / in.)} \\ \theta_{R,H} = \delta_{R,M} &= \frac{r_2}{\bar{r}} \theta_{R,M} \left( \sqrt{a^2 - \bar{r}^2} - \sqrt{a^2 - r_2^2} \right) = 15.66 \times 10^{-7} \text{ rad / (lb/in.)} \\ &\text{or in. / ((lb-in.) / in.)} \end{aligned} \right\} (B4a)$$

From reference 5, the shell influence coefficients for  $\varphi_2 = 0.1414$  radian are

$$\left. \begin{aligned} \delta_{S,H} &= -59.909 \times 10^{-7} \text{ in. / (lb/in.)} \\ \delta_{S,M} &= 652.79 \times 10^{-7} \text{ in. / ((lb-in.) / in.)} \\ \delta_{S,p} &= 28.489 \times 10^{-7} \text{ in. / psi} \\ \theta_{S,H} &= 652.79 \times 10^{-7} \text{ rad / (lb/in.)} \\ \theta_{S,M} &= -20321 \times 10^{-7} \text{ rad / ((lb-in.) / in.)} \\ \theta_{S,p} &\equiv 0 \end{aligned} \right\} (B4b)$$

Substitution of equations (B3) and (B4) into (B1b) yields the following discontinuity force and couple:

$$\left. \begin{aligned} H_1 &= 0.3339 p \\ M_1 &= 0.009353 p \end{aligned} \right\} (B5)$$

Finally, the elastic stress-concentration factor for the dome is

$$\frac{\sigma_{\max}}{\sigma_{\text{mem}}} = \frac{\frac{pa}{2h} + \frac{H_2 \cos \varphi_2}{h} + \frac{6M_2}{h^2}}{\frac{pa}{2h}} = 1.420 p \quad (\text{B6})$$

## APPENDIX C

### ELASTIC-PLASTIC MEMBRANE ANALYSIS

The first step in the calculation of stresses, strains, and dimensions in the membrane region of the spherical dome (table I) is the conversion of uniaxial tensile test data to true effective stress as a function of conventional strain. If  $A$  and  $A_0$  represent the instantaneous and original cross-sectional areas, respectively, of the tensile specimen, then

$$A = A_0(1 + \epsilon_t)^2$$

in which the subscript  $t$  denotes the transverse direction. If the material is assumed to be incompressible in both the elastic and the plastic states, the true uniaxial stress becomes

$$\bar{\sigma}_u = \sigma_u \frac{A_0}{A} = \frac{\sigma_u}{(1 - \epsilon_u/2)^2}$$

TABLE I. - CALCULATION OF MEMBRANE DIMENSIONS AND BURST PRESSURE

Uniaxial tensile data		True effective stress, $\bar{\sigma}_e$ , psi	Effective plastic strain, $\epsilon_{ep}$ , in./in.	Effective total strain, $\epsilon_{et}$ , in./in.	Elastic circumferential strain, $\epsilon_{\theta e}$ , in./in.	Plastic circumferential strain, $\epsilon_{\theta p}$ , in./in.	Total circumferential strain, $\epsilon_{\theta}$ , in./in.	Total transverse strain, $\epsilon_{\xi}$ , in./in.	Dome radius, a, in.	Dome wall thickness, h, in.	Internal pressure, p, lb/sq in.
Conventional stress, $\sigma_u$ , psi	Conventional strain, $\epsilon_u$ , in./in.										
36 000	0.00360	36 100	0	0.00321	0.00241	0	0.00241	-0.00241	6.044	0.0599	716
38 000	.00395	38 200	.00013	.00353	.00255	.00006	.00261	-.00268	6.046	.0598	756
40 000	.00470	40 200	.00068	.00425	.00268	.00034	.00302	-.00336	6.048	.0598	795
42 000	.00595	42 300	.00173	.00549	.00281	.00086	.00367	-.00454	6.052	.0597	835
44 000	.00830	44 400	.00386	.00781	.00296	.00193	.00489	-.00682	6.059	.0596	873
46 000	.0172	46 800	.0125	.0167	.00312	.00625	.00937	-.0156	6.087	.0591	909
48 000	.0323	49 600	.0273	.0317	.00331	.0136	.0169	-.0306	6.132	.0582	941
49 000	.0429	51 100	.0378	.0423	.00341	.0189	.0223	-.0412	6.164	.0575	953
50 000	.0560	52 800	.0507	.0554	.00352	.0254	.0289	-.0542	6.204	.0567	965
50 300	.0614	53 400	.0561	.0609	.00356	.0280	.0316	-.0597	6.220	.0564	968
50 500	.0668	53 900	.0614	.0662	.00359	.0307	.0343	-.0650	6.237	.0561	<sup>a</sup> 969
50 700	.0770	54 600	.0715	.0764	.00364	.0358	.0394	-.0759	6.268	.0555	967

<sup>a</sup>Membrane burst pressure.

Since equation (A4c) shows that the effective stress is equal to the nonzero stress in a uniaxial stress state, with second-order strain terms neglected, the true effective stress becomes

$$\bar{\sigma}_e = \sigma_u(1 + \epsilon_u) \quad (C1)$$

The effective plastic strain  $\epsilon_{ep}$  is calculated in accordance with the first part of equation (A1b). The true value of  $\sigma_u$ , namely  $\bar{\sigma}_e$ , is used because plastic flow in the true stress - conventional strain state is to be calculated. Next, the effective total strain  $\epsilon_{et}$  is obtained by using the second part of equation (A1b) with the constants  $\nu$  and  $E$  evaluated as 0.333 and  $10^7$  pounds per square inch, respectively.

The elastic component of the circumferential strain  $\epsilon_{\theta e}$  is assumed to obey Hooke's law, which, for a membrane sphere, is

$$\epsilon_{\theta e} = \frac{1 - \nu}{E} \sigma_\theta = 0.667 \frac{\bar{\sigma}_e}{10^7} \quad (C2)$$

The plastic component of the circumferential strain  $\epsilon_{\theta p}$  is calculated by equations (A1a) and (A2b). Since  $\epsilon_\theta = \epsilon_\varphi$  in a membrane sphere

$$\epsilon_{et} = \frac{2}{3} (\epsilon_\theta - \epsilon_\zeta)$$

which leads to

$$\epsilon_{\theta p} = \frac{\epsilon_{ep}}{2} \quad (C3)$$

The total circumferential strain  $\epsilon_\theta$  is equal to the sum of the elastic and plastic components.

The transverse strain  $\epsilon_\zeta$  is calculated from equation (A3). For a membrane sphere, equation (A3) becomes

$$\epsilon_\zeta = \frac{-2}{1 - \nu} \left[ \nu \epsilon_\theta + (1 - 2\nu) \epsilon_{\theta p} \right]$$

or, for  $\nu = 1/3$ ,

$$\epsilon_\zeta = -(\epsilon_{\theta e} + \epsilon_{ep}) \quad (C4)$$

The instantaneous values of the radius and wall thickness in a membrane region of the sphere are calculated as follows:

$$a = a_0(1 + \epsilon_\theta) = 6.03(1 + \epsilon_\theta) \quad (C5)$$

and

$$h = h_0(1 + \epsilon_\zeta) = 0.060(1 + \epsilon_\zeta) \quad (C6)$$

Finally, the internal pressures that produce the calculated stress and strain states are calculated by the equilibrium equation

$$p = 2 \frac{\bar{\sigma} h}{a} \quad (C7)$$

## REFERENCES

1. Kaufman, Albert, Bizon, Peter T., and Morgan, William C.: Investigation of Circular Reinforcements of Rectangular Cross Section Around Central Holes in Flat Sheets Under Biaxial Loads in the Elastic Range. NASA TN D-1195, 1962.
2. Kaufman, Albert, Bizon, Peter T., and Morgan, William C.: Investigation of Tapered Circular Reinforcements Around Central Holes in Flat Sheets under Biaxial Loads in the Elastic Range. NASA TN D-1101, 1962.
3. Beskin, L.: Strengthening of Circular Holes in Plates Under Edge Loads. Jour. Appl. Mech., vol. 11, no. 3, Sept. 1944, pp. A140-A148.
4. Galletly, G. D.: Influence Coefficients for Hemispherical Shells with Small Openings at the Vertex. Jour. Appl. Mech., vol. 21, no. 1, Mar. 1955, pp. 20-24.
5. Greszczuk, L. B.: Effect of Reinforcement Geometry on the Stresses in Spherical Shells. Paper 578C, SAE, 1962.
6. Hardrath, Herbert F., and Ohman, Lachlan: A Study of Elastic and Plastic Stress Concentration Factors Due to Notches and Fillets in Flat Plates. NACA TN 2566, 1951.
7. Stern, Perry: Elastic-Plastic Analysis of Shells of Revolution by a Finite Difference Method. Rep. LMSD-288183, Lockheed Aircraft Corp., Jan. 1960.
8. Stern, Perry: Stresses and Displacements in Elastic-Plastic Shells of Revolution with Temperature Dependent Properties. Rep. 6-90-62-123, Lockheed Missiles and Space Co., Jan. 1963.
9. Spera, David A: Analysis of Elastic-Plastic Shells of Revolution Containing Discontinuities. AIAA Jour., vol. 1, no. 11, Nov. 1963, pp. 2583-2589.
10. Calvert, Howard F., and Kemp, Richard H.: Determination of Pressure Vessel Strengths at  $-423^{\circ}$  F as Influenced by Notches of Various Radii. Paper 520B, SAE, 1962.
11. Timoshenko, S.: Strength of Materials. Third ed., pt. II, D. Van Nostrand Co., Inc., 1956, pp. 140 and 210.
12. Mendelson, A., and Manson, S. S.: Practical Solution of Plastic Deformation Problems in Elastic-Plastic Range. NASA TR R-28, 1959. (Supersedes NACA TN 4088.)

*"The aeronautical and space activities of the United States shall be conducted so as to contribute . . . to the expansion of human knowledge of phenomena in the atmosphere and space. The Administration shall provide for the widest practicable and appropriate dissemination of information concerning its activities and the results thereof."*

—NATIONAL AERONAUTICS AND SPACE ACT OF 1958

## NASA SCIENTIFIC AND TECHNICAL PUBLICATIONS

**TECHNICAL REPORTS:** Scientific and technical information considered important, complete, and a lasting contribution to existing knowledge.

**TECHNICAL NOTES:** Information less broad in scope but nevertheless of importance as a contribution to existing knowledge.

**TECHNICAL MEMORANDUMS:** Information receiving limited distribution because of preliminary data, security classification, or other reasons.

**CONTRACTOR REPORTS:** Technical information generated in connection with a NASA contract or grant and released under NASA auspices.

**TECHNICAL TRANSLATIONS:** Information published in a foreign language considered to merit NASA distribution in English.

**TECHNICAL REPRINTS:** Information derived from NASA activities and initially published in the form of journal articles.

**SPECIAL PUBLICATIONS:** Information derived from or of value to NASA activities but not necessarily reporting the results of individual NASA-programmed scientific efforts. Publications include conference proceedings, monographs, data compilations, handbooks, sourcebooks, and special bibliographies.

*Details on the availability of these publications may be obtained from:*

SCIENTIFIC AND TECHNICAL INFORMATION DIVISION  
NATIONAL AERONAUTICS AND SPACE ADMINISTRATION  
Washington, D.C. 20546